Biomaterials 243 (2020) 119942

Contents lists available at ScienceDirect

Biomaterials

journal homepage: www.elsevier.com/locate/biomaterials

Mesenchymal stem cell-derived magnetic extracellular nanovesicles for targeting and treatment of ischemic stroke

Han Young Kim[a,b,1], Tae Jung Kim[c,1], Lami Kang[c], Young-Ju Kim[c], Min Kyoung Kang[c], Jonghoon Kim[b,d], Ju Hee Ryu[a], Taeghwan Hyeon[b,d], Byung-Woo Yoon[c], Sang-Bae Ko[c,**], Byung-Soo Kim[b,e,f,*]

[a] Biomedical Research Institute, Korea Institute of Science and Technology, Seoul, 02792, Republic of Korea
[b] School of Chemical and Biological Engineering, Seoul National University, Seoul, 08826, Republic of Korea
[c] Department of Neurology, Seoul National University Hospital, Seoul, 03080, Republic of Korea
[d] Center for Nanoparticle Research, Institute for Basic Science (IBS), Seoul, 08826, Republic of Korea
[e] Interdisciplinary Program of Bioengineering, Seoul National University, Seoul, 08826, Republic of Korea
[f] Institute of Chemical Processes, Seoul National University, Seoul, 08826, Republic of Korea

ARTICLE INFO

Keywords:
Extracellular nanovesicles
Exosomes
Iron oxide nanoparticles
Mesenchymal stem cells
Ischemic stroke

ABSTRACT

Exosomes and extracellular nanovesicles (NV) derived from mesenchymal stem cells (MSC) may be used for the treatment of ischemic stroke owing to their multifaceted therapeutic benefits that include the induction of angiogenesis, anti-apoptosis, and anti-inflammation. However, the most serious drawback of using exosomes and NV for ischemic stroke is the poor targeting on the ischemic lesion of brain after systemic administration, thereby yielding a poor therapeutic outcome. In this study, we show that magnetic NV (MNV) derived from iron oxide nanoparticles (IONP)-harboring MSC can drastically improve the ischemic-lesion targeting and the therapeutic outcome. Because IONP stimulated expressions of therapeutic growth factors in the MSC, MNV contained greater amounts of those therapeutic molecules compared to NV derived from naive MSC. Following the systemic injection of MNV into transient middle-cerebral-artery-occlusion (MCAO)-induced rats, the magnetic navigation increased the MNV localization to the ischemic lesion by 5.1 times. The MNV injection and subsequent magnetic navigation promoted the anti-inflammatory response, angiogenesis, and anti-apoptosis in the ischemic brain lesion, thereby yielding a considerably decreased infarction volume and improved motor function. Overall, the proposed MNV approach may overcome the major drawback of the conventional MSC-exosome therapy or NV therapy for the treatment of ischemic stroke.

1. Introduction

Ischemic stroke is one of the most lethal diseases and is a leading cause of long-term disability [1]. The main pathological event of ischemic stroke is brain ischemia caused by blood-vessel occlusion and subsequent neuronal damage of the brain tissue [2]. The severe inflammation also contributes to the exacerbation of the neuronal injury and brain dysfunction [3]. The oxidative stress caused by ischemia and reperfusion in the brain tissue activates macrophages, thereby releasing proinflammatory cytokines that leads to a detrimental inflammation in the brain microenvironment [4,5].

The administration of mesenchymal stem cells (MSC) has attracted widespread attention for the treatment of cerebral ischemic stroke [6–8]. MSC have a large potential for the treatment of ischemic stroke because they release therapeutic biomolecules that induce angiogenesis [9], anti-apoptosis [10,11], and immunomodulation [12]. However, the difficulty to deliver MSC to the stroke lesion limits their clinical use for the treatment of cerebral ischemic stroke. The intracerebral implantation to the ischemic brain is invasive and may cause an additional damage to normal brain tissues [13]. Intravenous administration is simpler and less invasive in comparison with direct implantation. However, it leads to a large entrapment of MSC in the lung and poor accumulation

* Corresponding author. School of Chemical and Biological Engineering, Seoul National University, Seoul, 08826, Republic of Korea.
** Corresponding author. Department of Neurology, Seoul National University Hospital, Seoul, 03080, Republic of Korea.
E-mail addresses: sangbai1378@gmail.com (S.-B. Ko), byungskim@snu.ac.kr (B.-S. Kim).
[1] These authors contributed equally to this study.

https://doi.org/10.1016/j.biomaterials.2020.119942
Received 6 September 2019; Received in revised form 28 February 2020; Accepted 4 March 2020
Available online 06 March 2020
0142-9612/

in the ischemic brain. Owing to the large diameters of the MSC (15–40 μm), the pulmonary capillary acts as a barrier that captures intravenously infused MSC [14–16]. Furthermore, although a small amount of MSC may accumulate in the ischemic lesion in brain after systemic infusion, MSC exhibit poor survival in inflammatory and hypoxic condition [17].

MSC-derived exosomes may overcome the problems of MSC therapy for the treatment of ischemic stroke. Exosomes are extracellular vesicles (50–150 nm) that contain various mRNAs, microRNAs and proteins originated from the parent cells [18]. Nanometer-sized exosomes can pass the pulmonary capillaries and avoid accumulation in the lung following the systemic infusion [19]. Because exosomes are not live cells, the low efficacy of the MSC therapy due to the poor survival can be overcome by the MSC-derived exosome therapy. Furthermore, the autologous MSC therapy may not be ideal for patients who require emergency medical treatments because it is time-consuming to expand the autologous MSC *in vitro* prior to the implantation. In contrast, exosomes prepared using allogeneic MSC can serve as an off-the-shelf therapeutic agent owing to their low immunogenicity [20,21].

MSC-derived exosomes have been studied as therapeutic agents for the treatment of ischemic stroke [22–24]. Previous studies demonstrated that MSC-derived exosomes exhibit similar or equivalent therapeutic functions to those of MSC in the treatment of ischemic stroke. However, the poor *in vivo* targeting ability of systemically administered exosomes toward the ischemic stroke lesion is still a critical challenge [25–27]. The surface modification of the exosome with the Arg-Gly-Asp (RGD) peptide can enhance the accumulation of MSC-derived exosomes in the ischemic brain [24]. However, the conjugation of the RGD peptide requires multiple chemical reaction steps that may affect the functions of the exosomal proteins.

Although the MSC-derived exosome therapy can be advantageous over the MSC therapy for the treatment of ischemic stroke, the small quantities of exosomes released from MSC may limit the clinical application. Less than 4 μg of exosomes is produced by one million MSC per day [28], thereby indicating that the collection of a sufficient amount of exosomes for clinical studies is impractical and laborious. The culture of MSC in three-dimensional (3D) spheroids and incubating under a hypoxic condition can improve the exosome production efficiency by two and six times, respectively [29,30]. Moreover, a previous study demonstrated exosome-mimetic NV prepared by extruding cells through serial nano-porous membranes [31]. The NV prepared using embryonic stem cells with the extrusion method exhibited a 250-fold increased production yield compared to that of naturally secreted exosomes [32]. Therefore, NV are advantageous over exosomes in terms of clinical-scale production.

To obtain NV with a good targeting ability, we prepared magnetic nanovesicles (MNV) using IONP-harbored MSC (MSC-IONP) (Fig. 1). MNV contain IONP that mediate their magnetic navigation to the target ischemic lesion in the brain with the assistance of an external magnetic field (MF). The IONP are biocompatible because they can be assimilated by the body through ionization into iron ions and iron homeostasis (storage of excess iron ions in the form of ferritin) [33]. IONP (e.g., ferumoxytol) are approved by the Food and Drug Administration for the treatment of iron-deficiency anemia [34]. On the other hand, according to our previous studies, IONP can activate the phosphorylation of c-Jun and c-Jun N-terminal kinase (JNK) molecules [35,36], signaling cascades associated with growth factor expressions [37,38]. Through this mechanism, the expressions of therapeutic growth factors are considerably up-regulated in MSC-IONP. The MNV, fabricated by the serial extrusion of MSC-IONP, contain significantly larger amounts of therapeutic growth factors than those of the control NV prepared using untreated MSC. We synthesized MSC-derived NV having the brain ischemic lesion-targeting ability and larger amounts of therapeutic molecules, and demonstrated that the MNV exhibit significant therapeutic effect in treatment of ischemic stroke.

2. Materials and methods

2.1. Cell culture

Human-bone-marrow-derived MSC (Lonza, Switzerland) with passage numbers of 5–7 and rBMDM were cultured with a high-glucose Dulbecco's modified Eagle's medium (DMEM, Gibco, NY) supplemented with a 10% (v/v) fetal bovine serum (FBS), penicillin (100 units/mL), and streptomycin (100 μg/mL). HUVEC (Lonza) were cultured in 200PRF (Gibco) supplemented with a low-serum growth supplement (Gibco) consisting of 2% FBS (v/v), hydrocortisone (1 μg/mL), human epidermal growth factor (10 ng/mL), FGF2 (3 ng/mL), and heparin (10 μg/mL). PC12 cells (Paragon Biotech, Baltimore, MD) were cultured in RPMI 1640 (Gibco) supplemented with a 7.5% (v/v) FBS, 7.5% (v/v) horse serum, and 1% (v/v) penicillin/streptomycin. PC12 cells were treated with NGF (100 ng/mL) for neuronal differentiation.

2.2. IONP synthesis

IONP, having sizes of 12 nm, were synthesized through thermal decomposition of an iron oleate complex using a previously reported method [39]. The iron oleate complex was prepared by mixing 40 mmol of iron chloride and 120 mmol of sodium oleate into a solution containing 80 mL of ethanol, 60 mL of distilled water, and 140 mL of hexane. The resulting solution was heated up to 70 °C for 4 h. The upper organic layer was separated and washed several times with distilled water. Upon the evaporation of the organic solvent, the iron oleate complex was obtained for the synthesis of IONP. To synthesize the 12-nm IONP, 40 mmol of the as-prepared iron oleate complex and 20 mmol of oleic acid were dissolved in 200 g of 1-octadecene. After degassing under vacuum, the mixture was heated up to 320 °C at a rate of 3.3 °C/min and aged for 30 min. The resulting product was cooled to room temperature and washed with ethanol several times.

2.3. Internalization of the IONP in the MSC

To evaluate the cytotoxicity of the IONP in MSC, IONP were added to the culture medium at concentrations of 5, 10, 20, 40, 80, and 160 μg/mL. The viabilities of the IONP-treated MSC were determined by the CCK-8 assay after 16 h of treatment. Based on the results of the CCK-8 assay, the MSC were treated with IONP at a concentration of 40 μg/mL in the following experiments. After the IONP treatment, the MSC were extensively washed three times with PBS. For the detection of internalized IONP, the MSC-IONP were visualized using TEM (LIBRA 120, Carl Zeiss, Germany). Prussian blue staining was carried out to observe the internalized IONP in MSC-IONP [40]. For the assessment of the time-dependent gene expression, the total RNA was isolated from MSC-IONP at 2, 24, and 48 h after the IONP treatment. The concentration of total RNA was measured using a NanoDrop spectrometer (ND-2000, NanoDrop Technologies, Wilmington, DE). For Western blot analysis, proteins were extracted from the cell lysate at 48 h after treatment of IONP. The total protein concentration of the lysate was determined by a Bradford assay. For inhibition of JNK and c-Jun signaling pathway, MSC were co-treated with 20 μM of SP600125 (Tocris Bioscience, UK), a selective inhibitor of JNK and c-Jun [41], and 40 μg/mL of IONP. After 48 h, MNV were isolated from those SP600125-treated MSC-IONP (SP-MNV) for analysis.

2.4. Preparation of MNV

To isolate MNV, MSC-IONP were obtained at 48 h after IONP-treatment, and centrifuged at 300 g for 5 min. Collected MSC-IONP were then resuspended in PBS at a concentration of 1×10^6 cells/mL. Next, cells were disrupted by ultrasonication and centrifuged at 1000 g for 10 min to remove nuclei. Supernatants were collected and serially

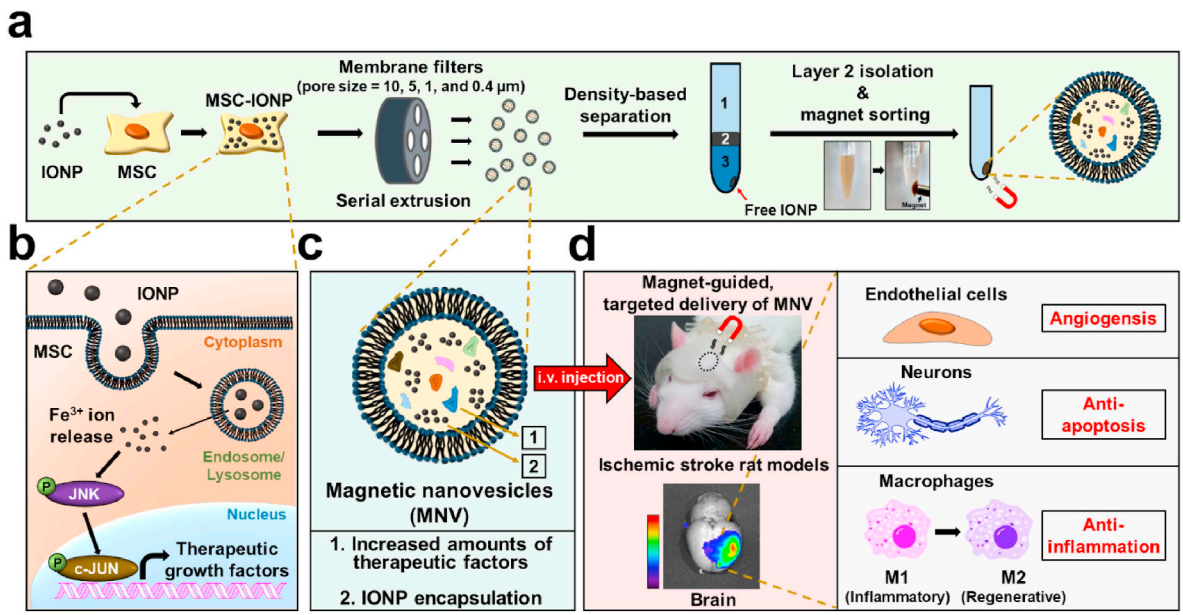

Fig. 1. Schematic illustration of the ischemic stroke treatment with MSC-derived magnetic nanovesicles (MNV). (a) Fabrication of MNV using IONP-harboring MSC (MSC-IONP). (b) Intracellular mechanism of the up-regulation of therapeutic growth factors in MSC-IONP. (c) MNV loaded with increased amounts of therapeutic factors and IONP. (d) Magnet-guided delivery of MNV to an ischemic stroke lesion in magnetic-helmet-wearing rats and therapeutic effects of the MNV on various cells (endothelial cells, neurons, and macrophages) in the ischemic lesion.

extruded through 10 μm, 5 μm, 1 μm, and 400 nm pore-sized membrane filters (Whatman, UK) using a mini-extruder (Avanti Polar Lipids, AL). For density-gradient ultracentrifugation, step gradient was formed using iodoxanol (OptiPrep, Axis-shield, UK). Iodoxanol (10% (v/v)) was carefully overlaid on top of 50% (v/v) iodoxanol. Extruded MSC-IONP were added to 10% (v/v) iodoxanol and ultracentrifuged at 100,000 g for 2 h. Subsequently, the MNV-enriched layer between 50% and 10% iodoxanol was collected and centrifuged again at 100,000 g for 2 h. Pellet was resuspended in PBS and magnetized using neodymium magnet to isolate MNV. SP-MNV were isolated from SP600125-treated MSC-IONP. NV were fabricated from naive MSC with the same protocol except for the magnetic separation. Fabricated NV and MNV were visualized using TEM. The total protein concentration of NV and MNV was determined by a Bradford assay. The size and number of NV and MNV were determined using Nanosight (LM10, Malvern, UK). The amounts of EGF, FGF2, VEGF, and TGF-β in NV and MNV were determined using human angiogenesis ELISA strip profiling assay (Signosis, CA). The concentrations of growth factors were normalized by total protein concentrations of NV and MNV. For evaluation of RNA integrity, total RNAs extracted from MSC, MSC-IONP, NV, or MNV were loaded on 1.5% (w/v) agarose gel and the gel was run in 100 V for 40 min.

2.5. Preparation of rBMDM

To isolate rBMDM, bone marrow was collected from the femurs of a five-week-old male Sprague Dawley (SD) rat (Koatech, Gyunggi-do, Korea) [42]. Hind limbs of animals were collected and the muscle tissue was removed to expose the femur bones. The bones were then flushed with PBS using syringes to isolate bone marrow cells. After centrifugation, the collected bone marrow cells were differentiated to macrophages for 4 days in a differentiation medium composed of a high-glucose DMEM supplemented with 30% (v/v) L929 cell-conditioned medium, 15% (v/v) FBS, 5% (v/v) horse serum, and 1% (v/v) penicillin/streptomycin. A conditioned medium from the L929 cell culture was prepared by growing the cells in a high-glucose DMEM containing 10% (v/v) FBS and 1% (v/v) penicillin/streptomycin. After 4 days of incubation, the macrophage differentiation medium was discarded and adherent BMDMs were harvested using cell scrapers.

2.6. In vitro therapeutic effects of the MNV

To investigate the angiogenic effect, tube formation and proliferation assays were carried out using the HUVEC treated with IONP (0.68 μg/mL, iron content equal to that of the MNV), NV (40 μg/mL), or MNV (40 μg/mL). For the tube formation assay, HUVEC were stained with DiO for 30 min, washed three times with PBS, and seeded on Matrigel (Corning, NY)-coated 24-well plates. IONP, NV, or MNV were added into the culture. After 8 h of incubation, the capillary tube formation of the HUVEC was analyzed by fluorescence microscopy. The numbers of tubes and tube junctions were evaluated using more than five images of each well (n = 3 wells per group). The cell proliferation assay was carried out by determining the relative cell number in the culture for 72 h after the treatment with the IONP, NV, or MNV. The relative cell number was determined by a CCK-8 assay. For migration assay, HUVEC were scratched with yellow pipette tips and incubated with IONP, NV, or MNV. Cell-free area was quantified at 0, 8, and 24 h after incubation. To evaluate the angiogenic effect of SP-MNV, proliferation and migration assay were carried out by treatment with SP-MNV (40 μg/mL) to HUVEC. In migration assay using SP-MNV, cell-free area was quantified at 0, 24, and 48 h after incubation. To investigate the anti-apoptotic effects of the MNV, PC12 cells were treated with IONP (680 ng/mL), NV (40 μg/mL), or MNV (40 μg/mL) for 16 h. After washing with PBS, the PC12 cells were treated with LPS (5 μg/mL) and incubated under hypoxic conditions (1% O_2) for 24 h. The cells were then stained with fluorescein diacetate (FDA) and ethidium bromide (EB) to detect live and dead cells, respectively. For flow cytometry, cells were stained with annexin V-FITC and PI (Biolegend, CA). Stained PC12 cells were analyzed with FACSAria II instrument installed at the National Center for Inter-university Research Facilities. The cell viability was quantified through the CCK-8 assay and RNA was extracted for further analysis. The expressions of genes encoding Bcl-2 and Bax were evaluated using qRT-PCR. To evaluate the macrophage polarization, rBMDM were seeded on six-well plates, treated with LPS (400 ng/mL),

and incubated under hypoxic conditions (1% O_2) for 24 h. After the removal of the LPS, the cells were treated with IONP (680 ng/mL), NV (40 μg/mL), or MNV (40 μg/mL) for 16 h, followed by an extensive washing with PBS and replenishing with a fresh DMEM. After 48 h, the expressions of proinflammatory M1 and anti-inflammatory M2 markers were assessed by qRT-PCR.

2.7. MCAO ischemia-reperfusion models and experimental groups

Nine-week-old SD rats (male, 250–300 g, Koatech) were used in all experiments. All experimental procedures were performed according to the guidelines and with the approval of the Institutional Animal Care and Use Committee (IACUC) of the Biomedical Research Institute of the Seoul National University Hospital (IACUC number: 17-0116-C2A0). The focal ischemia-reperfusion model was developed using the left transient MCAO with the intraarterial thread occlusion method [43–46]. After 60 min of left MCAO, the thread was carefully removed for reperfusion and the wound was sutured. The body temperature was maintained at 37 ± 0.5 °C during the procedures using a heating blanket while rectally monitoring the temperature. The experimental models were categorized into three groups: transient MCAO with PBS, transient MCAO with MNV injection [MNV (MF-)], and magnet-helmeted transient MCAO with MNV injection [MNV (MF+)]. Immediately after the reperfusion, MNV (200 μg in 300 μL of PBS) or 300 μL of PBS were injected into the tail vein. The 200 μg dose of MNV was used, based on previous reports that performed intravenous administration of MSC-derived exosomes or MSC-derived nanovesicles *in vivo* [47–49]. In the MNV (MF+) group, the magnet helmet was applied for three days after the injection of the MNV to evaluate the effect of the targeted delivery. The magnet helmet (ProJet) was fabricated using a 3D printer and embedded with a neodymium magnet ($5 \times 10 \times 2\ mm^3$, 0.32 T) on the left part.

2.8. Ex-vivo bio-distribution and cellular localization of MNV

MCAO-induced rats ($n = 3$ animals for each group) were sacrificed 24 h after the intravenous injection of VivoTrack 680-labeled MNV (200 μg per animal). The distribution of the injected MNV in the brain, liver, lung, spleen, and kidney was evaluated using an epi-illumination fluorescence imaging system (IVIS Lumina II, PerkinElmer, MA, USA). For a histological analysis, isolated ischemic brain tissues were embedded in paraffin and 10-μm-thick coronal sections were prepared. Prussian blue staining was carried out to visualize irons, while a nuclear fast red solution was used for counter staining. To assess cellular uptake of MNV by specific cell type, DiI was used to track MNV. Two hundred microgram of MNV were intravenously administered to MCAO-induced rats and brain tissues were collected at 24 h after administration. Paraffin sections were prepared and processed using primary antibodies against vWF, MAP2, GFAP (Abcam, CA), F4/80 (Santacruz Biotech, CA), and TMEM119 (Novus Biologicals, CO).

2.9. Measurement of cerebral infarct volume

The rats were sacrificed three days after the transient left MCAO by a cardiac perfusion with saline, followed by 4% paraformaldehyde in 0.1 M of PBS. The brains were removed, cut into 30-μm-thick coronal sections, and mounted on glass slides. The infarct volume was evaluated using serial sections collected for TTC staining ($n = 11$ animals for each group). To measure the infarct volume, the ImageJ program (National Institutes of Health, Bethesda, MD) was employed to analyze the images of the TTC-stained sections.

2.10. Behavioral tests

For the evaluation of the functional recovery after the MNV administration, a forelimb-placing test was carried out 1, 3, 7, 14, 21, and 28 days after the transient MCAO by two investigators blinded to the groups ($n = 6$ for each group) [43,50]. It consisted of two limb-placing tasks for the assessment of the sensorimotor integration of the forelimb and hindlimb by responses to tactile and proprioceptive stimulations of rats. The following scores were used to detect the impairments of the forelimb and hindlimb: 0 points (when the rat performed normally), 1 point (if the rat performed with a delay of more than 2 s and/or incompletely), and 2 points (if the rat did not perform the task). Both sides of the body were tested. The rats having a score of 8 indicated the most severe neurological symptom; conversely, the rats with a score of 0 were normal.

2.11. Western blot and IHC analyses of the extracted brain tissue

SD rats ($n = 3$ animals for each group) were sacrificed and transcardially perfused three days after the transient MCAO. For the Western blot analysis, the retrieved brain tissues were homogenized (D1000, Benchmark Scientific, NJ) in 300 μL of a lysis buffer, incubated on ice for 1 h, and centrifuged at 14,000 g for 30 min. After the centrifugation, the protein concentration of the isolated supernatant was measured by the Bradford assay and the Western blot analysis was performed with primary antibodies against iNOS, nNOS, Arg-1, MAP2, TNF-α, IL-1β, Cox-2, and GFAP (Abcam, CA). For IHC analysis, the paraffin sections were blocked by incubating with a 0.5% bovine serum albumin/0.3% Triton-X and 10% normal serum in PBS for 1 h. Additionally, the sections were incubated with primary antibodies against Iba1, CD86, Arg-1, vWF, MAP2 (Abcam), MPO (Santa Cruz Biotech), or TMEM119 at 4 °C for 16 h. After washing, the sections were incubated with a fluorescent-dye-conjugated secondary antibody. The microscopic analyses were performed using a Leica DM5500B microscope (Leica Microsystems) and LAS-AF image acquisition software (Leica Microsystems, Rijswijk, Netherlands).

2.12. Statistical analysis

The *in vitro* and *in vivo* data are quantitatively presented as mean ± standard deviation. For *in vitro* experiments, values are representative of three independent experiments with three or more samples per group. For *in vivo* experiments, values are representative of three independent experiments with three or more animals per group. The *p*-values were calculated by the one-way or two-way analysis of variance with the Turkey's significant difference post-hoc test using the GraphPad Prism software. The values of $p < 0.05$ were considered statistically significant.

3. Results and discussion

3.1. IONP internalization into MSC and up-regulation of growth factors

We analyzed the biological effects of the IONP on the MSC. Human-bone-marrow-derived MSC were treated with PEGylated superparamagnetic IONP with sizes of 12 nm (Fig. 2a). Transmission electron microscopy (TEM) showed the IONP internalization into the MSC (Fig. 2a). Agglomerated IONP clusters (red arrows) were observed in the endosomes of MSC-IONP. To evaluate the cytotoxicity of the IONP, the MSC were treated with IONP at various concentrations of 5–160 μg/mL and incubated for 8 h (Fig. 2b). A cell counting kit 8 (CCK-8) assay showed that the IONP did not exhibit cytotoxicity up to a concentration of 80 μg/mL. Prussian blue staining showed that the MSC treated with an increased dose of IONP contained more IONP (Fig. 2c). A quantitative real-time polymerase chain reaction (qRT-PCR) analysis indicated that the IONP treatment stimulated mRNA expressions of various therapeutic molecules associated with angiogenesis (angiopoietin 1 (Ang-1), fibroblast growth factor 2 (FGF2), hepatocyte growth factor (HGF), vascular endothelial growth factor (VEGF), platelet-derived growth factor (PDGF), transforming growth factor (TGF)-β1, TGF-β3),

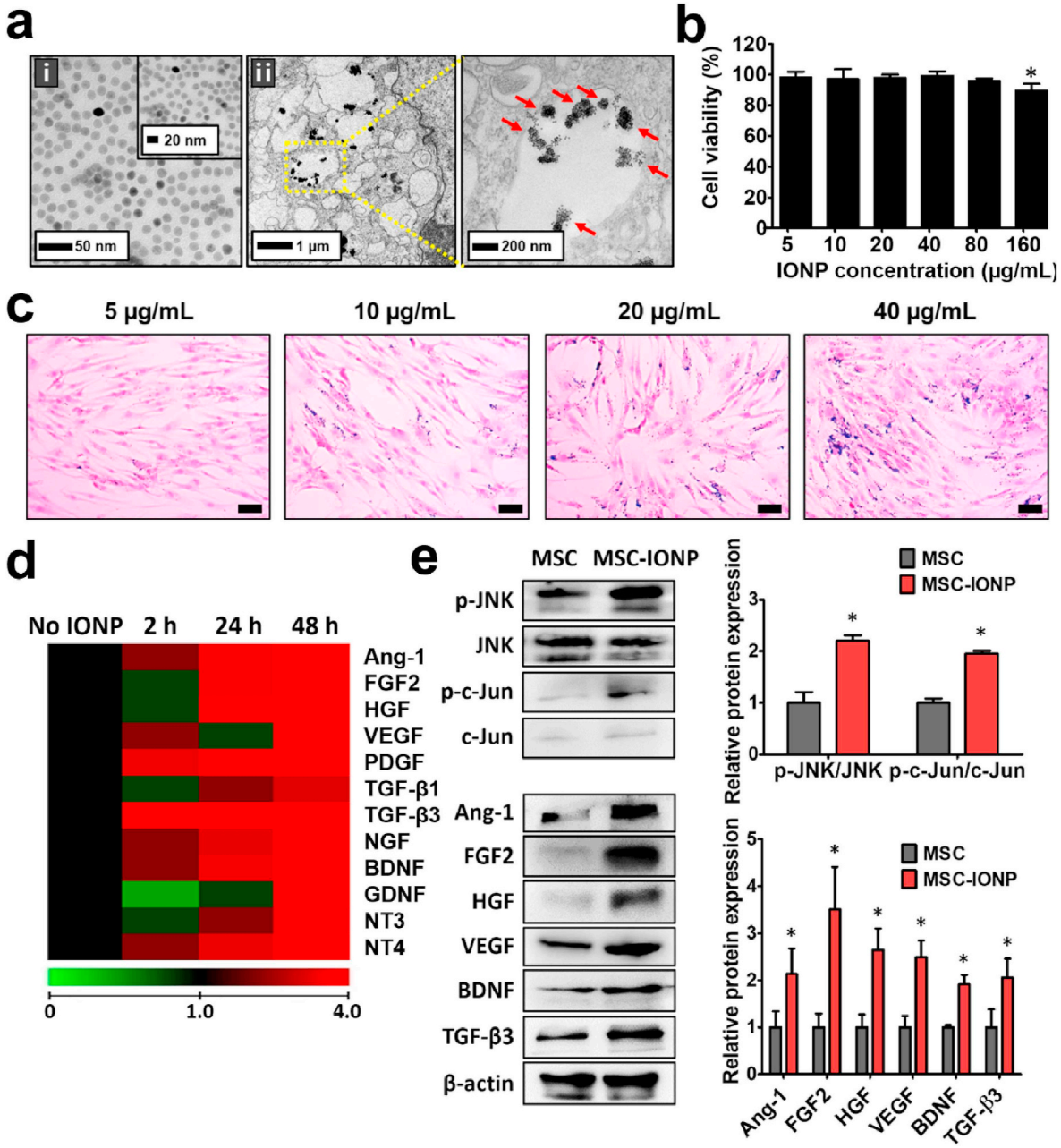

Fig. 2. Enhanced expressions of angiogenic, neuroprotective, and anti-inflammatory factors in the MSC by the IONP. (a) TEM images of the (i) IONP and (ii) MSC-IONP. The dotted yellow box indicates the endosome in MSC-IONP. (b) MSC viabilities at 16 h after the incubation with various concentrations of IONP. $^*P < 0.05$ versus no treatment ($n = 5$). (c) Dose-dependent uptake of IONP by the MSC, evaluated by the Prussian blue staining. The blue color indicates the IONP in the MSC. Scale bars = 100 μm. (d) Relative mRNA expressions of angiogenic (Ang-1, FGF2, HGF, VEGF, and PDGF), neuroprotective (NGF, BDNF, GDNF, NT3, and NT4), and anti-inflammatory (TGF-β1 and TGF-β3) factors in MSC-IONP 2, 24, and 48 h after the treatment with IONP, evaluated by the qRT-PCR analysis ($n = 3$). Western blotting and quantification of the (e) phosphorylated JNK, c-Jun, and angiogenic, neuroprotective, and anti-inflammatory factors in the MSC and MSC-IONP 48 h after the IONP treatment. $^*P < 0.05$ versus the MSC. In (d, e), the MSC were treated with IONP (40 μg/mL) ($n = 3$). (For interpretation of the references to color in this figure legend, the reader is referred to the Web version of this article.)

anti-apoptosis (FGF2, HGF, VEGF, PDGF, TGF-β1, TGF-β3), neurotrophic (nerve growth factor (NGF), brain-derived neurotrophic factor (BDNF), glial-cell-derived neurotrophic factor (GDNF), neurotrophin-3 (NT3), NT4), and anti-inflammation (TGF-β1, TGF-β3) factors in MSC-IONP (Fig. 2d). The low pH in the endosome induces a slow ionization of the IONP into iron ions [51], stimulating the JNK and c-Jun signaling (Figs. 1b and 2e). A Western blot analysis indicated that the protein expressions of Ang-1, FGF2, HGF, VEGF, BDNF, and TGF-β3 were significantly increased in MSC-IONP compared to those in the untreated MSC (Fig. 2e). Next, we investigated whether the enhanced expressions of the therapeutic molecules are attributed to the stimulated phosphorylation of JNK and c-Jun signaling molecules. MSC were co-treated with IONP and SP600125. After 48 h, phosphorylation of JNK and c-Jun and the expressions of therapeutic molecules were evaluated by Western blot (Fig. S1). SP600125 reduced the phosphorylation of JNK and c-Jun and the expressions of Ang-1, FGF2, HGF, and VEGF even in the presence of IONP.

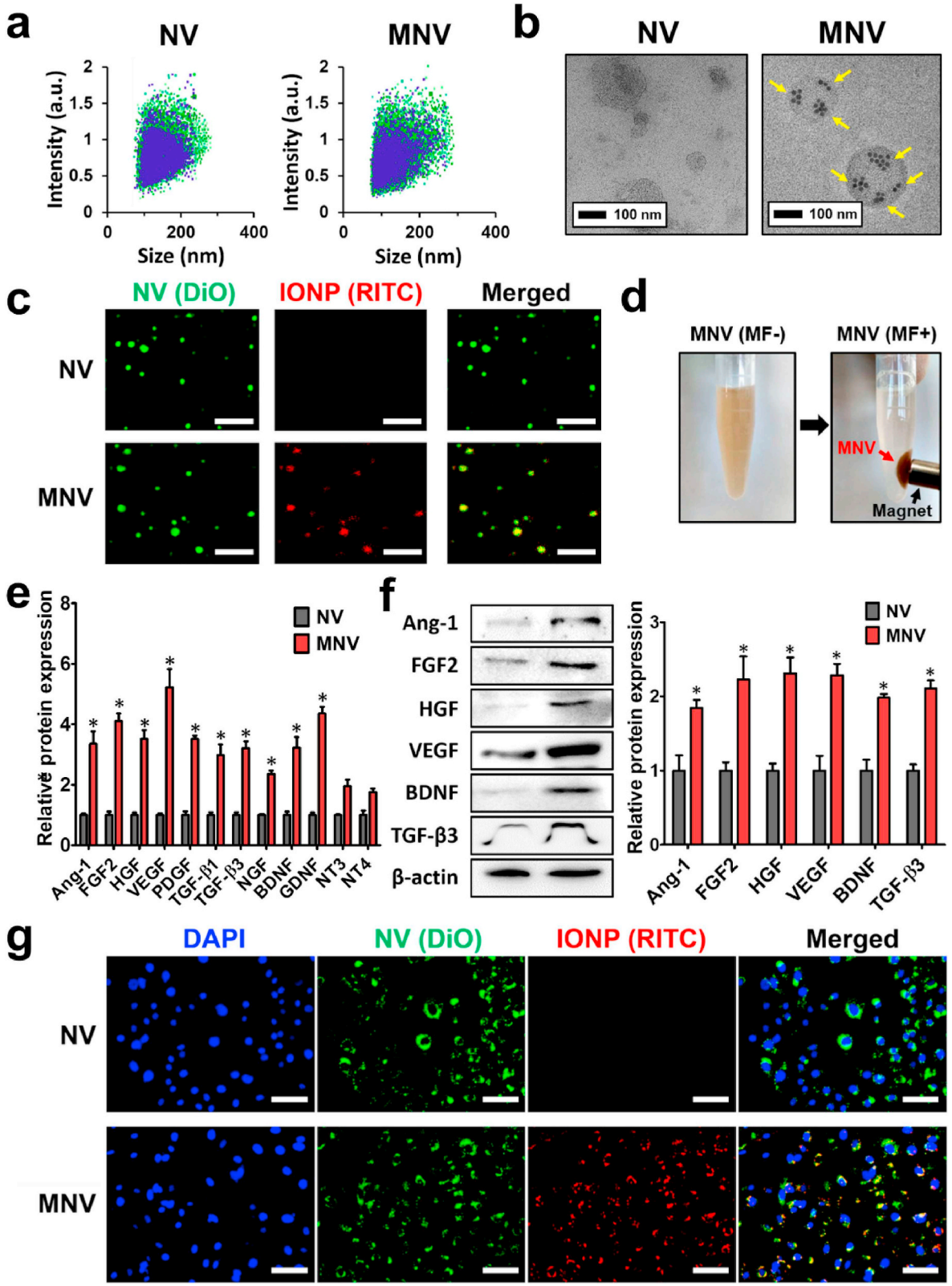

Fig. 3. Characterization of the NV and MNV. (a) Size distributions of the NV and MNV, evaluated by a nanoparticle tracking analysis. (b) TEM images of NV and MNV. The yellow arrows indicate IONP inside the MNV. (c) Fluorescence microscopy images of the NV and MNV. The lipid bilayers of the NV and MNV were stained with DiO (green), a lipophilic dye. RITC-labeled IONP were used for the synthesis of the MNV. Scale bars = 2 μm. (d) Attraction of MNV by magnetic field (MF). (e) qRT-PCR and (f) Western blot analyses of various therapeutic factors in the NV and MNV. *$P < 0.05$ versus the NV ($n = 3$). (g) NV and MNV uptakes by PC12 cells *in vitro*. The blue color indicates cell nuclei (DAPI). Scale bars = 50 μm. (For interpretation of the references to color in this figure legend, the reader is referred to the Web version of this article.)

3.2. Characterization of the MNV prepared using MSC-IONP

As the gene and protein expressions of the therapeutic growth factors were significantly enhanced in MSC-IONP 48 h after the IONP treatment, MSC-IONP were harvested 48 h after the treatment with IONP and serially extruded through membrane filters having pore sizes of 10, 5, 1, and 0.4 μm to obtain MNV. The NV prepared using the untreated MSC served as a control. A dynamic light scattering analysis showed that the NV and MNV had average sizes of 168.3 ± 48.3 and 194.2 ± 44.5 nm, respectively (Fig. 3a). Particle numbers of NV and MNV per 1 μg of protein were $10.2 \times 10^8 \pm 1.6 \times 10^8$, and $8.2 \times 10^8 \pm 0.5 \times 10^8$, respectively (Fig. S2). The TEM revealed spherical shapes and lipid bilayers in both NV and MNV and IONP (yellow arrows) encapsulated in the MNV (Fig. 3b). The encapsulation of IONP in the MNV was further confirmed by confocal microscopy. The MNV were fabricated using rhodamine-B-isothiocyanate (RITC, red)-labeled IONP. The lipid bilayers of the MNV were stained with 3,3′-dioctadecyloxacarbocyanine perchlorate (DiO, green). The confocal microscopy of the MNV revealed the overlapped locations of green and red fluorescence signals, indicating the encapsulation of IONP in the MNV (Fig. 3c). The MNV (dark-brown pellets) were attracted by a magnet (Fig. 3d). Further, we determined whether the larger amounts of the therapeutic molecules in MSC-IONP can be transferred to the MNV prepared using MSC-IONP. qRT-PCR (Fig. 3e) and Western blot (Fig. 3f) analyses showed that the MNV contained significantly larger amounts of the therapeutic mRNAs and proteins than those in the NV. Next, the amounts of therapeutic growth factors in NV and MNV relative to their protein concentrations were determined by ELISA (Fig. S3). It was revealed that MNV contained significantly larger amounts of therapeutic growth factors than NV. The amounts of EGF, FGF-2, VEGF, and TGF-β per 1 μg of NV were 84.3, 64.5, 410.4, and 31.1 pg, respectively. Meanwhile, the amounts of EGF, FGF2, VEGF, and TGF-β per 1 μg of MNV were 156.8, 171.1, 1225.6, and 58.1 pg, respectively. Following NV and MNV isolation through fierce extrusion, total RNAs in NV and MNV showed no significant changes in RNA integrity compared to their source cells, as determined by comparing the ratio of 28s/18s rRNA band intensity in agarose gel electrophoresis (Fig. S4) [52]. Next, pheochromocytoma 12 (PC12) cells, a neuronal cell line, were treated with NV and MNV. After 4 h, the NV and MNV were effectively up-taken by the cells (Fig. 3g). These results demonstrate that the MNV contained not only IONP as targeting agents but also significantly larger amounts of therapeutic factors exerting angiogenic, anti-apoptotic, and anti-inflammatory effects. In contrast, MNV isolated from SP600125-treated MSC-IONP (SP-MNV) contained lower amounts of therapeutic proteins compared to NV (Fig. S5).

3.3. In vitro enhanced angiogenesis, anti-apoptotic, and anti-inflammatory effects of the MNV

We investigated whether the MNV exerted enhanced angiogenic, anti-apoptotic, and anti-inflammatory effects *in vitro*. Human umbilical vein endothelial cells (HUVEC), neuron-like PC12 cells, and rat bone marrow-derived macrophages (rBMDM) were treated with NV (40 μg/mL), MNV (40 μg/mL), and IONP (0.68 μg/mL, equal concentrations of IONP in 40 μg/mL of MNV). The IONP served as a control to determine whether the therapeutic growth factors or IONP were the therapeutic sources of the MNV. The angiogenic activity of the HUVEC was determined by a tube formation assay after their treatment with IONP, NV, or MNV for 8 h (Fig. 4a). The capillary tube formation of HUVEC was prominent in the MNV group. The HUVEC treated with the MNV exhibited the most active proliferation (Fig. 4b) and migration (Fig. S6). These results may be attributed to the larger amounts of angiogenic factors such as Ang-1, FGF2, HGF, and VEGF in the MNV [53,54]. In this context, we also examined the angiogenic effect of SP-MNV. Proliferation and migration of HUVEC were assessed after treatment with SP-MNV (Fig. S7). Likely due to low amounts of angiogenic factors in SP-MNV, proliferation or migration of SP-MNV-treated HUVEC did not change.

Further, we determined whether the MNV exert anti-apoptotic and neuroprotective effects on the neuron-like PC12 cells under inflammatory and hypoxic conditions, typical in the brain microenvironment after an ischemic stroke [55]. Prior to assessments, PC12 cells were neuronally differentiated by treatment with NGF. NGF treatment induces PC12 cells to change the phenotype and acquire a number of properties of sympathetic neurons [56]. Differentiated PC12 cells cease to proliferate, extend neurite outgrowth, and can develop synapses with primary neurons [57,58]. To induce apoptosis, PC12 cells were treated with lipopolysaccharide (LPS, 5 μg/mL) and incubated under hypoxic (1% O_2) conditions [59,60]. The cells were pretreated with IONP, NV, or MNV before the induction of apoptosis. After 24 h, the PC12 cells treated with the MNV exhibited the highest cell survival rate (Fig. 4c). After the incubation of the PC12 cells under the inflammatory and hypoxic conditions, the early apoptotic cell population (annexin V-positive and propidium iodide (PI)-negative) and late apoptotic cell population (positive for both annexin V and PI) were increased to ~20% and ~25%, respectively (Fig. 4c). Surprisingly, the MNV treatment largely reduced the apoptotic cell populations to ~6% and ~9%, respectively. Compared to the other treatments, the MNV treatment significantly up-regulated the mRNA expression of the anti-apoptotic B-cell lymphoma-2 (Bcl-2) and down-regulated that of the proapoptotic Bcl-2-associated X-protein (Bax) (Fig. 4d). The MNV treatment significantly increased the viability of the PC12 cells compared to those after the IONP and NV treatments (Fig. 4e).

Further, we investigated the anti-inflammatory effect of the MNV. Macrophages can exist in proinflammatory and cytotoxic (M1) and anti-inflammatory and regenerative (M2) states [61]. During the progression of stroke, the M1 phenotype largely increases in the peri-infarct regions and releases proinflammatory cytokines, which exacerbate the neuronal injury [62]. The phenotypic transition of M1 macrophages toward the M2 subtype can prevent further brain damage [63]. To determine whether the MNV elicit M2 polarization of the M1 macrophages, the rBMDM were activated to the M1 state by an LPS treatment and culture under hypoxic conditions. The M1 phenotype-induced cells were then treated with IONP, NV, or MNV for 48 h, and the mRNA expressions of M1 macrophage markers (inducible nitric oxide synthase (iNOS), interleukin (IL)-1β, and tumor necrosis factor (TNF)-α) and M2 macrophage markers (arginase 1 (Arg-1), cluster of differentiation 206 (CD206), and IL-10) were evaluated (Fig. 4f). Compared to those of the nonactivated rBMDM (normoxia), the M1 macrophage-induced rBMDM (LPS/hypoxia) exhibited highly up-regulated expressions of the M1 markers. Notably, the MNV treatment significantly down-regulated the expressions of the M1 markers, while the M2 marker expressions were considerably increased. These results demonstrate that the MNV can elicit the M2 polarization of the M1-induced macrophages. Anti-inflammation and polarization of inflammatory M1 macrophages into regenerative M2 phenotype by MNV are likely attributed to the growth factors contained in MNV. VEGF induces polarization of M1 macrophages to M2 phenotype [64,65]. TGF-β has a pivotal role in immunosuppression [66]. TGF-β promotes M1 to M2 polarization *via* stimulation of SNAIL and down-regulation of NF-κB [67,68].

In these *in vitro* experiments, the IONP or SP-MNV treatment did not lead to significant differences from the control groups (nontreated group or LPS/hypoxia group). This demonstrates that the therapeutic effects of the MNV are attributed to the therapeutic growth factors rather than the incorporated IONP.

3.4. Targeted delivery of the MNV to an ischemic lesion

To evaluate the feasibility of a magnet-guided delivery of the MNV to an ischemic stroke lesion, the MNV were intravenously injected to transient middle cerebral artery occlusion (MCAO)-induced rats. To induce an external MF in the stroke lesion (left hemisphere (LH)) in the

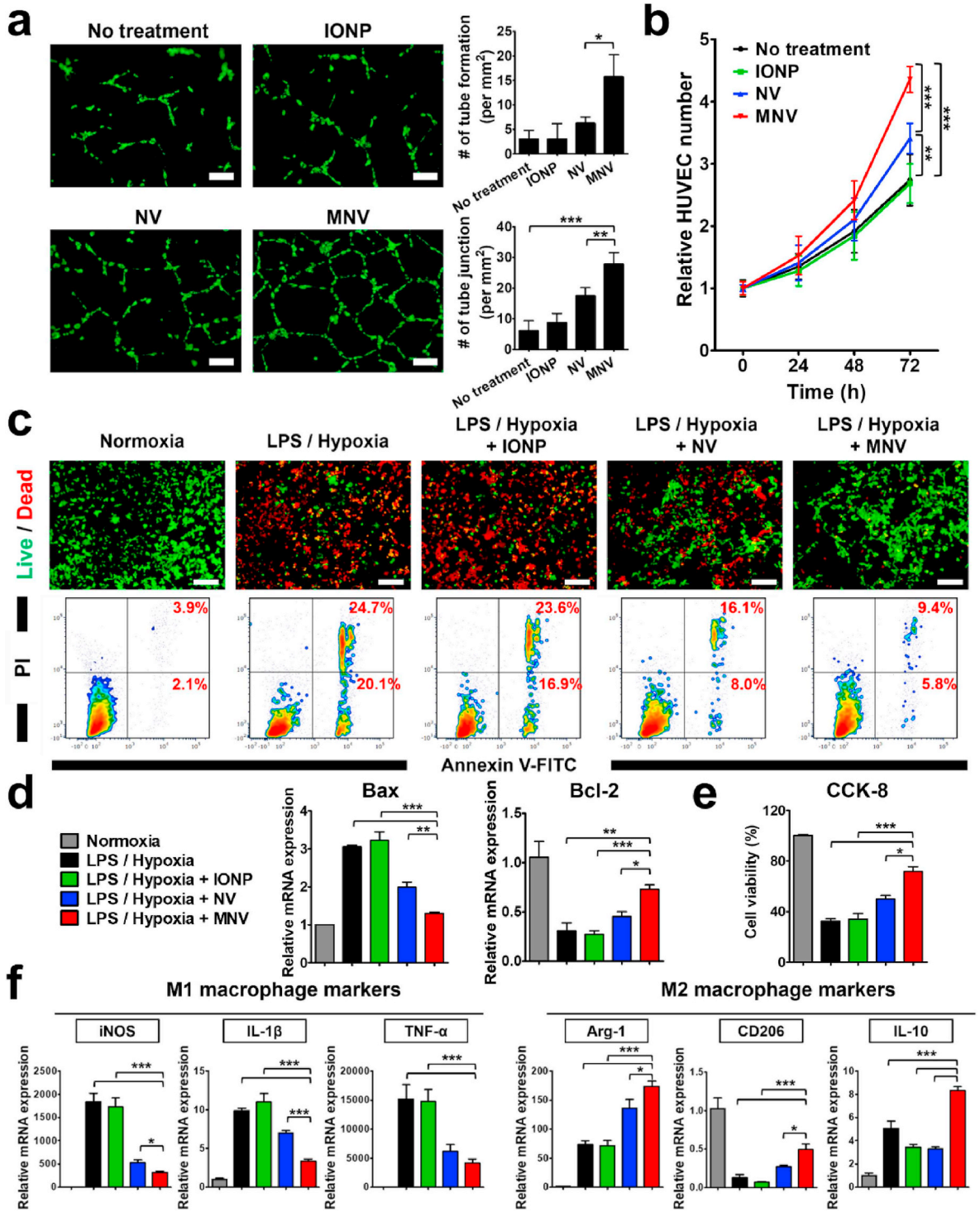

Fig. 4. *In vitro* angiogenic, neuroprotective, and anti-inflammatory effects of the NV and MNV on the endothelial cells (HUVEC), neuronal cells (PC12 cells), and macrophages (rBMDM). (a) Angiogenic behaviors of the HUVEC after the treatments with the IONP (0.68 μg/mL), NV (40 μg/mL), and MNV (40 μg/mL), determined by the tube formation assay. The HUVEC were stained with DiO, a green fluorescent dye. Scale bars = 100 μm. The numbers of tube formations and tube junctions were evaluated. (b) Proliferation of the HUVEC after various treatments, evaluated by the CCK-8 assay. (c) Viabilities and apoptotic behaviors of the PC12 cells treated with the IONP, NV, and MNV followed by incubation under inflammatory (LPS) and hypoxic (1% O_2) conditions. For the visualization of live and dead cells, the PC12 cells were stained with FDA (green) and EB (red), respectively. The apoptosis was evaluated by flow cytometry. The cells were double-stained with annexin V-FITC and PI. (d) Relative mRNA expressions of Bax (proapoptotic gene) and Bcl-2 (anti-apoptotic gene), evaluated by the qRT-PCR analysis. The normoxia group was not treated with LPS and hypoxia. (e) Viability of the PC12 cells evaluated by the CCK-8 assay. (f) Relative mRNA expressions of M1 (iNOS, IL-1β, and TNF-α) and M2 (Arg-1, CD206, and IL-10) macrophage markers in the rBMDM after the various treatments. The rBMDM were polarized to the M1 phenotype by the LPS treatment and hypoxia prior to the various treatments. (a, b, d–f) $^{*}P < 0.05$, $^{**}P < 0.01$, $^{***}P < 0.001$ ($n = 3$). (For interpretation of the references to color in this figure legend, the reader is referred to the Web version of this article.)

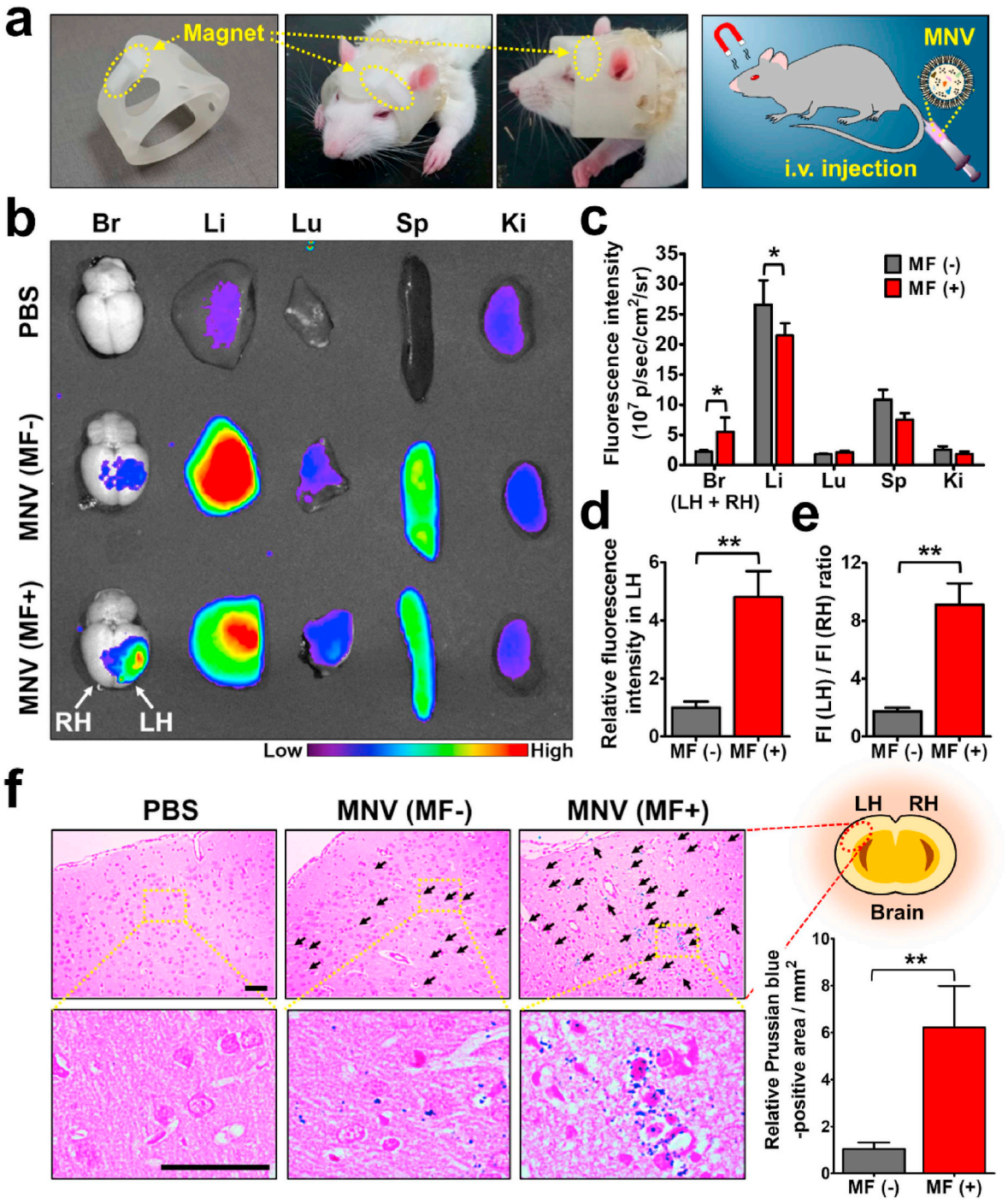

Fig. 5. *In vivo* targeted delivery of systemically injected MNV to the ischemic stroke lesion of the MCAO rat by the external MF. (a) 3D-printed magnetic helmet used for the magnetic navigation of the systemically injected MNV toward the ischemic stroke lesion. (b) Bio-distribution of the MNV following their intravenous injection (200 μg) into the MCAO-induced rat with or without the MF, evaluated by the IVIS imaging of major organs (Br: brain, Li: liver, Lu: lung, Sp: spleen, and Ki: kidney). LH: left hemisphere (ischemic lesion), RH: right hemisphere (non-ischemic region) (c) Quantification of the fluorescence intensities of the major organs. (d) Effect of the MF on the MNV localization in the LH (ischemic lesion). (e) Ischemic lesion-specific accumulation of MNV by the MF, indicated by the ratio of the fluorescence intensity (denoted as FI) in the LH to that in the RH. (f) Prussian blue staining of the ischemic stroke lesion in the LH following the MNV injection with or without the MF. The blue color (arrows) indicates the IONP in the MNV. Scale bars = 50 μm. The Prussian blue-positive area was quantified. (c–f) $^{*}P < 0.05$, $^{**}P < 0.01$ ($n = 3$ animals per group). (For interpretation of the references to color in this figure legend, the reader is referred to the Web version of this article.)

brain for magnetic navigation of the MNV, magnet helmets for rats were fabricated using a 3D printer and neodymium magnets were embedded in the magnet helmets (Fig. 5a). For *in vivo* fluorescence imaging, the MNV were fluorescently labeled with a lipophilic dye VivoTrack 680 prior to the injection. The fluorescence imaging 24 h after the injection revealed that without the MF (MF-), a small amount of MNV accumulated in the brain (Fig. 5b), likely owing to the disruption of the brain-blood barrier during the progression of the ischemic stroke [69]. The majority of the MNV were uptaken by the liver and spleen. This is in agreement with the previous studies, which demonstrated that systemically administered extracellular vesicles rapidly accumulate in organs of the reticuloendothelial system such as the liver and spleen

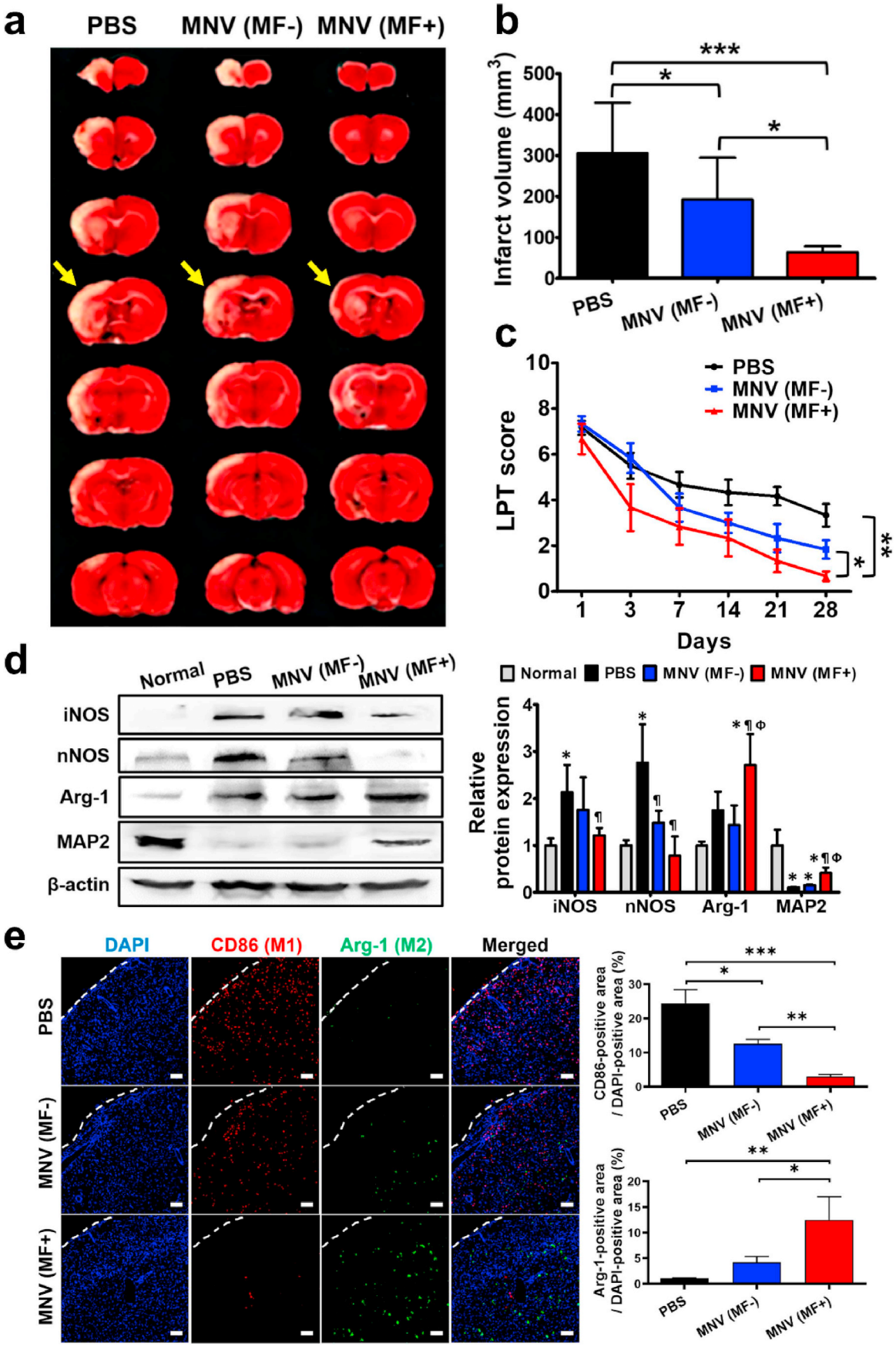

(caption on next page)

Fig. 6. *In vivo* therapeutic effect of the MNV on the ischemic stroke. MCAO rats were treated with the intravenous injection of either PBS, MNV (MF-), or MNV (MF+). (a) TTC staining of serial sections of the brain and (b) quantification of the cerebral infarction (arrows in the TTC staining) volume ($n = 11$ animals per group). (c) Brain functional recoveries of the MCAO rats evaluated by the limb placement test (LPT) ($n = 6$ animals per group). The rats with a score of 8 exhibited the most severe neurological symptom, while the rats with the score of 0 were normal. (d) Western blot analysis and quantification for M1 (iNOS and nNOS) and M2 (Arg-1) macrophage markers and neuronal marker (MAP2) in the brain tissues of the MCAO rats. The normal group did not receive MCAO. *, ¶, and Φ indicate significant differences ($P < 0.05$), compared to the normal, PBS, and MNV (MF-) groups, respectively. Staining for (e) M1 (CD86) and M2 (Arg-1) macrophages, (f) blood vessels (vWF), (g) neurons (MAP2), and (h) apoptotic cells (TUNEL) in the ischemic stroke lesion. The scale bars correspond to 50 μm in (e, f) and 100 μm in (g, h). (b–h) $*P < 0.05$, $**P < 0.01$, $***P < 0.001$, and (d–h) $n = 3$ animals per group.

[24,25,27]. Notably, the MF (MF+) considerably increased the fluorescence signals in the ischemic brain, particularly in the LH (ischemic lesion) where the MF was applied. A region-of-interest analysis revealed that the MF increased (2.9 times) the MNV accumulation in the brain compared to that without the MF (Fig. 5c). In the LH of the brain, the MF increased (5.1 times) the MNV accumulation compared to that without the MF (Fig. 5d). The increase in targeting efficiency toward the ischemic lesion is considerably higher than that of previously reported RGD-modified exosomes (~3-fold) [24]. The MF increased the fluorescence ratio of the LH to the right hemisphere (RH) to 9.2, which was 1.7 for the MF(−) group (Fig. 5e), demonstrating the ischemic lesion-specific accumulation of the MNV with the aid of the MF. The Prussian blue staining of the LH confirmed that the MF significantly increased the MNV accumulation in the ischemic lesion (Fig. 5f). Next, we investigated the cellular uptake of MNV by specific cell type in infarcted brain. MNV were fluorescently labeled with DiI and intravenously injected to MCAO-induced rats in presence of MF. After 24 h, brains were collected and IHC was performed to label various cell types (Fig. S8). In ischemic lesion, fluorescence signal from MNV was co-localized within von Willebrand factor (vWF)-stained endothelial cells. Furthermore, various cell types targeted by MNV were evaluated by staining for microtubule-associated protein 2 (MAP2, neuron marker), glial fibrillary acid protein (GFAP, astrocyte marker), F4/80 (macrophage marker), or TMEM119 (microglia marker). TMEM119, cell-surface protein selectively expressed by microglia, can distinguish microglia from infiltrating macrophages [70]. Observed with confocal microscopy, fluorescence signal from MNV was detected not only in endothelial cells, but also in neurons, astrocytes, macrophages, and microglia. This result is consistent with a previous study demonstrating the cellular localization of MSC-derived extracellular vesicles in various types of cells in infarcted brain [24,71]. Targeting ability of MNV to endothelial cells and neurons may attribute to VLA-4 and SNAP-25 proteins expressed on the MSC membrane, respectively [72,73]. Because reactive astrocytes, inflammatory macrophages, and activated microglia function as phagocytes after brain ischemia [74], MNV can be phagocytosized by those cell types. Cellular internalization of extracellular vesicles such as exosomes can occur through phagocytosis [75].

3.5. *In vivo* therapeutic effects of the MNV on the ischemic stroke

To investigate the therapeutic effects of the MNV on the ischemic stroke, we evaluated the infarct volume three days after the MCAO and injection of MNV (Fig. 6a). Brains were collected and stained with 2,3,5-triphenyltetrazolium chloride (TTC). The unstained tissues (yellow arrows) indicate the infarcted lesion. The infarct volume of the MNV (MF+) group was significantly smaller than those of the MNV (MF-) and phosphate-buffered saline (PBS) (Fig. 6b) groups. The infarct volume of the MNV (MF-) group was smaller than that of the PBS group possibly owing to the small accumulation of MNV in the ischemic lesion. These results showed that the MNV accumulation in the ischemic lesion reduced the infarct volume. A limb placement test (LPT) showed a fast functional recovery in the MNV (MF+) group (Fig. 6c).

Further, we investigated the therapeutic mechanisms of the MNV. Based on the *in vitro* findings, the anti-inflammatory, angiogenic, and neuroprotective effects were assessed. The Western blot analysis of brain tissue lysates showed that proinflammatory M1 markers such as iNOS and neuronal nitric oxide synthase (nNOS) were significantly attenuated in the MNV (MF+) group, compared to the other groups (Fig. 6d). The expressions of Arg-1 (M2 macrophage marker) and MAP2 in the MNV (MF+) group were significantly higher than those of the other groups. Other M1 macrophage markers (TNF-α, IL-1β, and Cox-2) and marker of reactive astrocytes such as GFAP were prominently attenuated in the MNV (MF+) group (Fig. S9). Full western blots in this study are shown in Fig. S10. IHC staining showed that the MNV (MF+) group exhibited a considerably attenuated expression of CD86 (M1) and increased expression of Arg-1 (M2), compared to those of the other groups (Fig. 6e). Because microglia mediate major immune responses in the central nervous system, we also investigated whether the activation of microglia is attenuated by MNV. We processed brain sections with anti-TMEM119 (microglia marker) and anti-Iba1 (activation marker) antibodies to evaluate the activation of microglia (Fig. S11). The IHC staining demonstrated that administration of MNV (MF+) markedly attenuated the microglia activation. Additionally, reduced expression of myeloperoxidase (MPO), an inflammation marker, was observed in the ischemic lesion (Fig. S12). These results indicate that the MNV accumulated in the ischemic lesion induced the polarization of brain-resident macrophages toward the M2 subtype and attenuated the microglia activation. The IHC staining for the vWF indicates that more blood vessels were observed in the MNV (MF+) group (Fig. 6f), demonstrating the promotion of angiogenesis by MNV. Moreover, the IHC staining for MAP2 showed that the MNV accumulated in the ischemic lesion exhibited an excellent neuroprotection, whereas the PBS group exhibited a severe neuronal loss (Fig. 6g). A terminal deoxynucleotidyl transferase deoxyuridine triphosphate nick-end labeling (TUNEL) staining of the ischemic lesion showed that the number of apoptotic cells in the ischemic lesion was considerably reduced by the administration of the MNV (MF+) (Fig. 6h).

4. Conclusion

This study demonstrated the feasibility of MSC-derived NV with magnetic properties for the treatment of ischemic stroke. The IONP-incorporated MSC exhibited enhanced expressions of therapeutic growth factors inducing angiogenesis, anti-apoptosis, and anti-inflammation. The MNV prepared using MSC-IONP contained large amounts of therapeutic growth factors and IONP. The magnetic properties generated by the IONP enabled the MNV to target the ischemic brain with the aid of the 3D-printed magnet helmet. The MNV accumulated in the ischemic brain improved the blood vessel density, elicited the macrophage polarization from the inflammatory M1 phenotype to the anti-inflammatory M2 phenotype, and consequently attenuated the neuronal damage in the infarcted lesion. Owing to these therapeutic effects, the MNV exhibited a significantly reduced infarction volume and improved motor function of the brain. Therefore, the MSC-derived NV therapy is feasible for the treatment of ischemic stroke.

CRediT authorship contribution statement

Han Young Kim: Conceptualization, Methodology, Investigation, Formal analysis, Writing - original draft. **Tae Jung Kim:** Methodology, Validation, Investigation, Writing - original draft. **Lami Kang:**

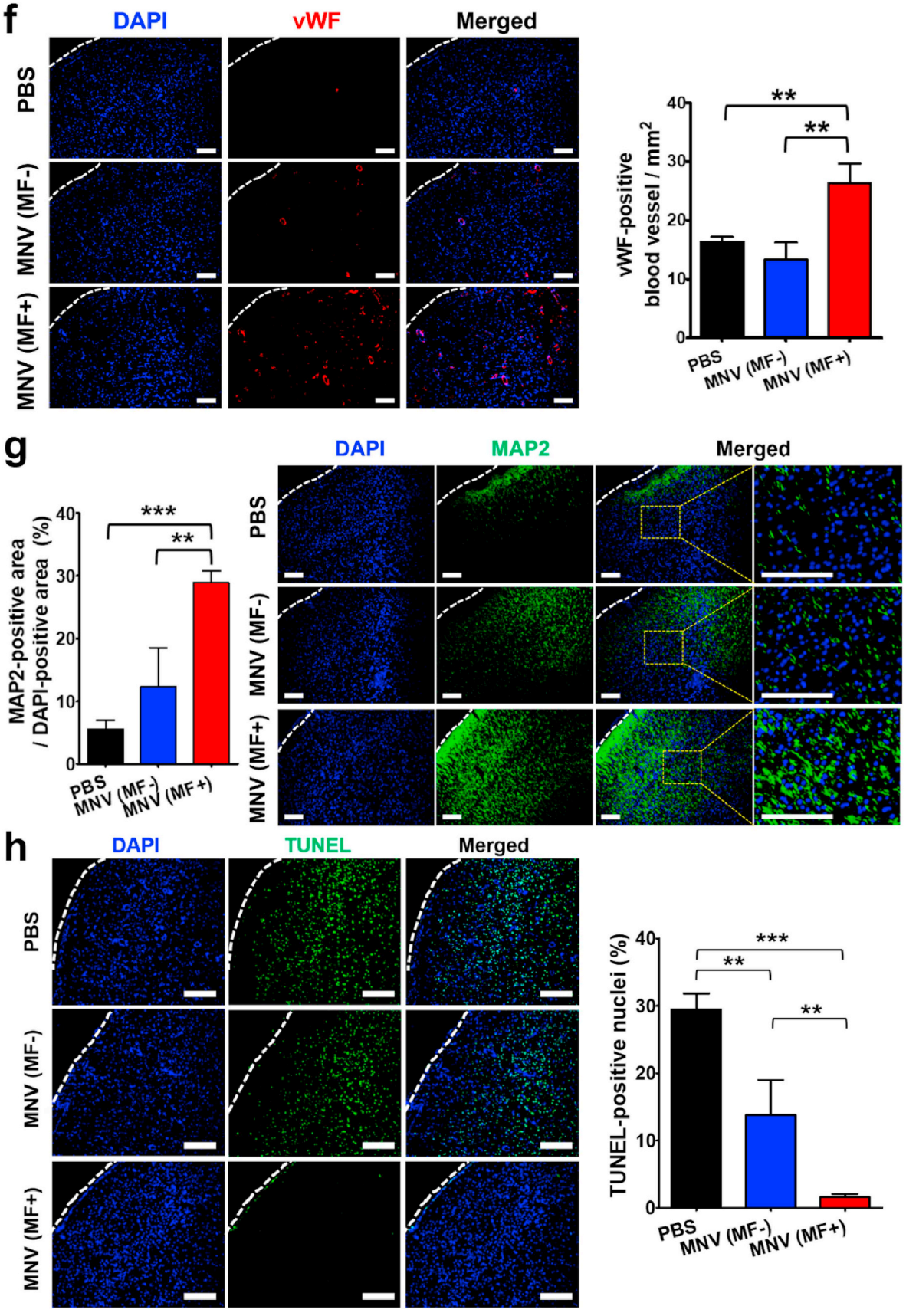

Fig. 6. (*continued*)

Investigation, Formal analysis. **Young-Ju Kim:** Investigation, Validation. **Min Kyoung Kang:** Investigation. **Jonghoon Kim:** Investigation, Resources. **Ju Hee Ryu:** Resources, Supervision. **Taeghwan Hyeon:** Resources, Supervision. **Byung-Woo Yoon:** Resources, Supervision. **Sang-Bae Ko:** Writing - review & editing, Supervision, Project administration, Funding acquisition. **Byung-Soo Kim:** Conceptualization, Writing - review & editing, Supervision, Project administration, Funding acquisition.

Declaration of competing interest

The authors declare no competing financial interest.

Acknowledgements

This study was supported by the Seoul National University Hospital (Grant No. 0420150840), National Research Foundation of Korea (2019M3A9H1103651), and Korea Health Industry Development Institute (HI18C0183) funded by the Ministry of Health and Welfare, Republic of Korea.

Appendix A. Supplementary data

Supplementary data to this article can be found online at https://doi.org/10.1016/j.biomaterials.2020.119942.

Data availability

The raw and processed data required to reproduce these findings will be available upon request.

References

[1] L.K. Chen, G.L. Zhang, A.A. Khan, X.Y. Guo, Y.C. Gu, Clinical efficacy and meta-analysis of stem cell therapies for patients with brain ischemia, Stem Cell. Int. 2016 (2016) 6129579.
[2] R.R. Moustafa, J.C. Baron, Pathophysiology of ischaemic stroke: insights from imaging, and implications for therapy and drug discovery, Br. J. Pharmacol. 153 (2008) S44–S54.
[3] R. Jin, G.J. Yang, G.H. Li, Inflammatory mechanisms in ischemic stroke: role of inflammatory cells, J. Leukoc. Biol. 87 (5) (2010) 779–789.
[4] C. Iadecola, J. Anrather, The immunology of stroke: from mechanisms to translation, Nat. Med. 17 (7) (2011) 796–808.
[5] B. Becher, S. Spath, J. Goverman, Cytokine networks in neuroinflammation, Nat. Rev. Immunol. 17 (1) (2017) 49–59.
[6] G.H. Li, F.B. Yu, T. Lei, H.J. Gao, P.W. Li, Y.X. Sun, H.Y. Huang, Q.C. Mu, Bone marrow mesenchymal stem cell therapy in ischemic stroke: mechanisms of action and treatment optimization strategies, Neural Regen Res 11 (6) (2016) 1015–1024.
[7] O.Y. Bang, E.H. Kim, J.M. Cha, G.J. Moon, Adult stem cell therapy for stroke: challenges and progress, J Stroke 18 (3) (2016) 256–266.
[8] Y.J. Cho, H.S. Song, S. Bhang, S. Lee, B.G. Kang, J.C. Lee, J. An, C.I. Cha, D.H. Nam, B.S. Kim, K.M. Joo, Therapeutic effects of human adipose stem cell-conditioned medium on stroke, J. Neurosci. Res. 90 (9) (2012) 1794–1802.
[9] T. Zhang, Y.W. Lee, Y.F. Rui, T.Y. Cheng, G. Li, Bone marrow-derived mesenchymal stem cells promote angiogenesis and growth of breast and prostate tumors, Cytotherapy 15 (4) (2013) S15-S15.
[10] Y. Gu, Y. Zhang, Y. Bi, J.J. Liu, B. Tan, M. Gong, T.Y. Li, J. Chen, Mesenchymal stem cells suppress neuronal apoptosis and decrease IL-10 release via the TLR2/NF kappa B pathway in rats with hypoxic-ischemic brain damage, Mol. Brain 8 (2015).
[11] S.H. Bhang, Y.E. Lee, S.W. Cho, J.W. Shim, S.H. Lee, C.Y. Choi, J.W. Chang, B.S. Kim, Basic fibroblast growth factor promotes bone marrow stromal cell transplantation-mediated neural regeneration in traumatic brain injury, Biochem. Biophys. Res. Commun. 359 (1) (2007) 40–45.
[12] R. Zhang, Y. Liu, K. Yan, L. Chen, X.R. Chen, P. Li, F.F. Chen, X.D. Jiang, Anti-inflammatory and immunomodulatory mechanisms of mesenchymal stem cell transplantation in experimental traumatic brain injury, J. Neuroinflammation 10 (2013).
[13] W.C. Shyu, S.Z. Lin, M.F. Chiang, C.Y. Su, H. Li, Intracerebral peripheral blood stem cell (CD34(+)) implantation induces neuroplasticity by enhancing beta 1 integrin-mediated angiogenesis in chronic stroke rats, J. Neurosci. 26 (13) (2006) 3444–3453.
[14] J. Boltze, A. Arnold, P. Walczak, J. Jolkkonen, L. Cui, D.C. Wagner, The dark side of the force - constraints and complications of cell therapies for stroke, Front. Neurol. 6 (2015) 155.
[15] R.H. Lee, A.A. Pulin, M.J. Seo, D.J. Kota, J. Ylostalo, B.L. Larson, L. Semprun-Prieto, P. Delafontaine, D.J. Prockop, Intravenous hMSCs improve myocardial infarction in mice because cells embolized in lung are activated to secrete the anti-inflammatory protein TSG-6, Cell Stem Cell 5 (1) (2009) 54–63.
[16] U.M. Fischer, M.T. Harting, F. Jimenez, W.O. Monzon-Posadas, H. Xue, S.I. Savitz, G.A. Laine, C.S. Cox Jr., Pulmonary passage is a major obstacle for intravenous stem cell delivery: the pulmonary first-pass effect, Stem Cell. Dev. 18 (5) (2009) 683–692.
[17] E. Eggenhofer, F. Luk, M.H. Dahlke, M.J. Hoogduijn, The life and fate of mesenchymal stem cells, Front. Immunol. 5 (2014) 148.
[18] G. Raposo, W. Stoorvogel, Extracellular vesicles: exosomes, microvesicles, and friends, J. Cell Biol. 200 (4) (2013) 373–383.
[19] T. Smyth, M. Kullberg, N. Malik, P. Smith-Jones, M.W. Graner, T.J. Anchordoquy, Biodistribution and delivery efficiency of unmodified tumor-derived exosomes, J. Contr. Release 199 (2015) 145–155.
[20] X. Zhu, M. Badawi, S. Pomeroy, D.S. Sutaria, Z. Xie, A. Baek, J. Jiang, O.A. Elgamal, X. Mo, K. Perle, J. Chalmers, T.D. Schmittgen, M.A. Phelps, Comprehensive toxicity and immunogenicity studies reveal minimal effects in mice following sustained dosing of extracellular vesicles derived from HEK293T cells, J. Extracell. Vesicles 6 (1) (2017) 1324730.
[21] B. Zhang, R.W.Y. Yeo, R.C. Lai, E.W.K. Sim, K.C. Chin, S.K. Lim, Mesenchymal stromal cell exosome-enhanced regulatory T-cell production through an antigen-presenting cell-mediated pathway, Cytotherapy 20 (5) (2018) 687–696.
[22] G.E. Manuel, T. Johnson, D. Liu, Therapeutic angiogenesis of exosomes for ischemic stroke, Int J Physiol Pathophysiol Pharmacol 9 (6) (2017) 188–191.
[23] H. Xin, Y. Li, Y. Cui, J.J. Yang, Z.G. Zhang, M. Chopp, Systemic administration of exosomes released from mesenchymal stromal cells promote functional recovery and neurovascular plasticity after stroke in rats, J. Cerebr. Blood Flow Metabol. 33 (11) (2013) 1711–1715.
[24] T. Tian, H.X. Zhang, C.P. He, S. Fan, Y.L. Zhu, C. Qi, N.P. Huang, Z.D. Xiao, Z.H. Lu, B.A. Tannous, J. Gao, Surface functionalized exosomes as targeted drug delivery vehicles for cerebral ischemia therapy, Biomaterials 150 (2018) 137–149.
[25] O.P. Wiklander, J.Z. Nordin, A. O'Loughlin, Y. Gustafsson, G. Corso, I. Mager, P. Vader, Y. Lee, H. Sork, Y. Seow, N. Heldring, L. Alvarez-Erviti, C.I. Smith, K. Le Blanc, P. Macchiarini, P. Jungebluth, M.J. Wood, S.E. Andaloussi, Extracellular vesicle in vivo biodistribution is determined by cell source, route of administration and targeting, J. Extracell. Vesicles 4 (2015) 26316.
[26] D.W. Hwang, H. Choi, S.C. Jang, M.Y. Yoo, J.Y. Park, N.E. Choi, H.J. Oh, S. Ha, Y.S. Lee, J.M. Jeong, Y.S. Gho, D.S. Lee, Noninvasive imaging of radiolabeled exosome-mimetic nanovesicle using Tc-99m-HMPAO, Sci Rep-Uk 5 (2015).
[27] C.P. Lai, O. Mardini, M. Ericsson, S. Prabhakar, C. Maguire, J.W. Chen, B.A. Tannous, X.O. Breakefield, Dynamic biodistribution of extracellular vesicles in vivo using a multimodal imaging reporter, ACS Nano 8 (1) (2014) 483–494.
[28] T. Katsuda, R. Tsuchiya, N. Kosaka, Y. Yoshioka, K. Takagaki, K. Oki, F. Takeshita, Y. Sakai, M. Kuroda, T. Ochiya, Human adipose tissue-derived mesenchymal stem cells secrete functional neprilysin-bound exosomes, Sci. Rep. 3 (2013) 1197.
[29] M. Kim, H.W. Yun, D.Y. Park, B.H. Choi, B.H. Min, Three-dimensional spheroid culture increases exosome secretion from mesenchymal stem cells, Tissue Eng Regen Med 15 (4) (2018) 427–436.
[30] C. Salomon, J. Ryan, L. Sobrevia, M. Kobayashi, K. Ashman, M. Mitchell, G.E. Rice, Exosomal signaling during hypoxia mediates microvascular endothelial cell migration and vasculogenesis, PloS One 8 (7) (2013) e68451.
[31] S.C. Jang, O.Y. Kim, C.M. Yoon, D.S. Choi, T.Y. Roh, J. Park, J. Nilsson, J. Lotvall, Y.K. Kim, Y.S. Gho, Bioinspired exosome-mimetic nanovesicles for targeted delivery of chemotherapeutics to malignant tumors, ACS Nano 7 (9) (2013) 7698–7710.
[32] W. Jo, J. Kim, J. Yoon, D. Jeong, S. Cho, H. Jeong, Y.J. Yoon, S.C. Kim, Y.S. Gho, J. Park, Large-scale generation of cell-derived nanovesicles, Nanoscale 6 (20) (2014) 12056–12064.
[33] J. Kolosnjaj-Tabi, L. Lartigue, Y. Javed, N. Luciani, T. Pellegrino, C. Wilhelm, D. Alloyeau, F. Gazeau, Biotransformations of magnetic nanoparticles in the body, Nano Today 11 (3) (2016) 280–284.
[34] M. Auerbach, G.M. Chertow, M. Rosner, Ferumoxytol for the treatment of iron deficiency anemia, Expet Rev. Hematol. 11 (10) (2018) 829–834.
[35] J. Han, B. Kim, J.Y. Shin, S. Ryu, M. Noh, J. Woo, J.S. Park, Y. Lee, N. Lee, T. Hyeon, D. Choi, B.S. Kim, Iron oxide nanoparticle-mediated development of cellular gap junction crosstalk to improve mesenchymal stem cells' therapeutic efficacy for myocardial infarction, ACS Nano 9 (3) (2015) 2805–2819.
[36] H.Y. Kim, H. Kumar, M.J. Jo, J. Kim, J.K. Yoon, J.R. Lee, M. Kang, Y.W. Choo, S.Y. Song, S.P. Kwon, T. Hyeon, I.B. Han, B.S. Kim, Therapeutic efficacy-potentiated and diseased organ-targeting nanovesicles derived from mesenchymal stem cells for spinal cord injury treatment, Nano Lett. 18 (8) (2018) 4965–4975.
[37] M.M. Vleugel, A.E. Greijer, R. Bos, E. van der Wall, P.J. van Diest, c-Jun activation is associated with proliferation and angiogenesis in invasive breast cancer, Hum. Pathol. 37 (6) (2006) 668–674.
[38] L. Shi, Y. Chang, Y. Yang, Y. Zhang, F.S. Yu, X. Wu, Activation of JNK signaling mediates connective tissue growth factor expression and scar formation in corneal wound healing, PloS One 7 (2) (2012) e32128.
[39] J. Park, K. An, Y. Hwang, J.G. Park, H.J. Noh, J.Y. Kim, J.H. Park, N.M. Hwang, T. Hyeon, Ultra-large-scale syntheses of monodisperse nanocrystals, Nat. Mater. 3 (12) (2004) 891–895.
[40] P.J. Chen, Y.D. Kang, C.H. Lin, S.Y. Chen, C.H. Hsieh, Y.Y. Chen, C.W. Chiang, W. Lee, C.Y. Hsu, L.D. Liao, C.T. Fan, M.L. Li, W.C. Shyu, Multitheragnostic multi-GNRs crystal-seeded magnetic nanoseaurchin for enhanced in vivo mesenchymal-stem-cell homing, multimodal imaging, and stroke therapy, Adv. Mater. 27 (41) (2015) 6488–6495.
[41] B.L. Bennett, D.T. Sasaki, B.W. Murray, E.C. O'Leary, S.T. Sakata, W. Xu, J.C. Leisten, A. Motiwala, S. Pierce, Y. Satoh, S.S. Bhagwat, A.M. Manning,

D.W. Anderson, SP600125, an anthrapyrazolone inhibitor of Jun N-terminal kinase, Proc. Natl. Acad. Sci. U. S. A. 98 (24) (2001) 13681–13686.
[42] G. Boltznitulescu, C. Wiltschke, C. Holzinger, A. Fellinger, O. Scheiner, A. Gessl, O. Forster, Differentiation of rat bone-marrow cells into macrophages under the influence of mouse L929 cell supernatant, J. Leukoc. Biol. 41 (1) (1987) 83–91.
[43] C.K. Kim, X.L. Yang, Y.J. Kim, I.Y. Choi, H.G. Jeong, H.K. Park, D. Kim, T.J. Kim, H. Jang, S.B. Ko, B.W. Yoon, Effect of long-term treatment with fimasartan on transient focal ischemia in rat brain, BioMed Res. Int. 2015 (2015) 295925.
[44] E.Z. Longa, P.R. Weinstein, S. Carlson, R. Cummins, Reversible middle cerebral-artery occlusion without craniectomy in rats, Stroke 20 (1) (1989) 84–91.
[45] M. Song, Y.J. Kim, Y.H. Kim, J. Roh, E.C. Kim, H.J. Lee, S.U. Kim, B.W. Yoon, Long-term effects of magnetically targeted ferumoxide-labeled human neural stem cells in focal cerebral ischemia, Cell Transplant. 24 (2) (2015) 183–190.
[46] M. Song, Y.J. Kim, Y.H. Kim, J. Roh, S.U. Kim, B.W. Yoon, Using a neodymium magnet to target delivery of ferumoxide-labeled human neural stem cells in a rat model of focal cerebral ischemia, Hum. Gene Ther. 21 (5) (2010) 603–610.
[47] J.H. Huang, X.M. Yin, Y. Xu, C.C. Xu, X. Lin, F.B. Ye, Y. Cao, F.Y. Lin, Systemic administration of exosomes released from mesenchymal stromal cells attenuates apoptosis, inflammation, and promotes angiogenesis after spinal cord injury in rats, J. Neurotrauma 34 (24) (2017) 3388–3396.
[48] Y. Zhao, X. Sun, W. Cao, J. Ma, L. Sun, H. Qian, W. Zhu, W. Xu, Exosomes derived from human umbilical cord mesenchymal stem cells relieve acute myocardial ischemic injury, Stem Cell. Int. 2015 (2015) 761643.
[49] A. Farinazzo, S. Angiari, E. Turano, E. Bistaffa, S. Dusi, S. Ruggieri, R. Bonafede, R. Mariotti, G. Constantin, B. Bonetti, Nanovesicles from adipose-derived mesenchymal stem cells inhibit T lymphocyte trafficking and ameliorate chronic experimental autoimmune encephalomyelitis, Sci. Rep. 8 (1) (2018) 7473.
[50] M. De Ryck, J. Van Reempts, M. Borgers, A. Wauquier, P.J.S. Janssen, Photochemical stroke model: flunarizine prevents sensorimotor deficits after neocortical infarcts in rats, 20 (10) (1989) 1383–1390.
[51] F. Mazuel, A. Espinosa, N. Luciani, M. Reffay, R. Le Borgne, L. Motte, K. Desboeufs, A. Michel, T. Pellegrino, Y. Lalatonne, C. Wilhelm, Massive intracellular biodegradation of iron oxide nanoparticles evidenced magnetically at single-endosome and tissue levels, ACS Nano 10 (8) (2016) 7627–7638.
[52] N.A. Skrypina, A.V. Timofeeva, G.L. Khaspekov, L.P. Savochkina, R.S. Beabealashvilli, Total RNA suitable for molecular biology analysis, J. Biotechnol. 105 (1–2) (2003) 1–9.
[53] J.E. Nor, J. Christensen, D.J. Mooney, P.J. Polverini, Vascular endothelial growth factor (VEGF)-mediated angiogenesis is associated with enhanced endothelial cell survival and induction of Bcl-2 expression, Am. J. Pathol. 154 (2) (1999) 375–384.
[54] M. Saito, M. Hamasaki, M. Shibuya, Induction of tube formation by angiopoietin-1 in endothelial cell/fibroblast co-culture is dependent on endogenous VEGF, Canc. Sci. 94 (9) (2003) 782–790.
[55] Q. Wang, X.N. Tang, M.A. Yenari, The inflammatory response in stroke, J. Neuroimmunol. 184 (1–2) (2007) 53–68.
[56] K.P. Das, T.M. Freudenrich, W.R. Mundy, Assessment of PC12 cell differentiation and neurite growth: a comparison of morphological and neurochemical measures, Neurotoxicol. Teratol. 26 (3) (2004) 397–406.
[57] T. Zhou, B.N. Xu, H.P. Que, Q.X. Lin, S.H. Lv, S.J. Liu, Neurons derived from PC12 cells have the potential to develop synapses with primary neurons from rat cortex, Acta Neurobiol. Exp. 66 (2) (2006) 105–112.
[58] A.L. Hughes, L. Gollapudi, T.L. Sladek, K.E. Neet, Mediation of nerve growth factor-driven cell cycle arrest in PC12 cells by p53. Simultaneous differentiation and proliferation subsequent to p53 functional inactivation, J. Biol. Chem. 275 (48) (2000) 37829–37837.
[59] S.L. Dholakiya, K.E. Benzeroual, Protective effect of diosmin on LPS-induced apoptosis in PC12 cells and inhibition of TNF-alpha expression, Toxicol. Vitro 25 (5) (2011) 1039–1044.
[60] M. He, H. Sun, J. Pang, X. Guo, Y. Huo, X. Wu, Y. Liu, J. Ma, Propofol alleviates hypoxia-induced nerve injury in PC-12 cells by up-regulation of microRNA-153, BMC Anesthesiol. 18 (1) (2018) 197.
[61] F.O. Martinez, S. Gordon, The M1 and M2 paradigm of macrophage activation: time for reassessment, F1000Prime Rep 6 (2014) 13.
[62] X. Hu, P. Li, Y. Guo, H. Wang, R.K. Leak, S. Chen, Y. Gao, J. Chen, Microglia/macrophage polarization dynamics reveal novel mechanism of injury expansion after focal cerebral ischemia, Stroke 43 (11) (2012) 3063–3070.
[63] Y. Zheng, R. He, P. Wang, Y. Shi, L. Zhao, J. Liang, Exosomes from LPS-stimulated macrophages induce neuroprotection and functional improvement after ischemic stroke by modulating microglial polarization, Biomater Sci 7 (5) (2019) 2037–2049.
[64] K.C. Wheeler, M.K. Jena, B.S. Pradhan, N. Nayak, S. Das, C.D. Hsu, D.S. Wheeler, K. Chen, N.R. Nayak, VEGF may contribute to macrophage recruitment and M2 polarization in the decidua, PloS One 13 (1) (2018).
[65] O.R. Colegio, N.Q. Chu, A.L. Szabo, T. Chu, A.M. Rhebergen, V. Jairam, N. Cyrus, C.E. Brokowski, S.C. Eisenbarth, G.M. Phillips, G.W. Cline, A.J. Phillips, R. Medzhitov, Functional polarization of tumour-associated macrophages by tumour-derived lactic acid, Nature 513 (7519) (2014) 559–563.
[66] A. Yoshimura, G. Muto, TGF-beta function in immune suppression, Curr. Top. Microbiol. Immunol. 350 (2011) 127–147.
[67] F. Zhang, H. Wang, X. Wang, G. Jiang, H. Liu, G. Zhang, H. Wang, R. Fang, X. Bu, S. Cai, J. Du, TGF-beta induces M2-like macrophage polarization via SNAIL-mediated suppression of a pro-inflammatory phenotype, Oncotarget 7 (32) (2016) 52294–52306.
[68] R.A. Flavell, S. Sanjabi, S.H. Wrzesinski, P. Licona-Limon, The polarization of immune cells in the tumour environment by TGFbeta, Nat. Rev. Immunol. 10 (8) (2010) 554–567.
[69] A. Kassner, Z. Merali, Assessment of blood-brain barrier disruption in stroke, Stroke 46 (11) (2015) 3310–3315.
[70] M.L. Bennett, F.C. Bennett, S.A. Liddelow, B. Ajami, J.L. Zamanian, N.B. Fernhoff, S.B. Mulinyawe, C.J. Bohlen, A. Adil, A. Tucker, I.L. Weissman, E.F. Chang, G. Li, G.A. Grant, M.G.H. Gephart, B.A. Barres, New tools for studying microglia in the mouse and human CNS, P Natl Acad Sci USA 113 (12) (2016) E1738–E1746.
[71] N. Perets, O. Betzer, R. Shapira, S. Brenstein, A. Angel, T. Sadan, U. Ashery, R. Popovtzer, D. Offen, Golden exosomes selectively target brain pathologies in neurodegenerative and neurodevelopmental disorders, Nano Lett. 19 (6) (2019) 3422–3431.
[72] L. Zachar, D. Bacenkova, J. Rosocha, Activation, homing, and role of the mesenchymal stem cells in the inflammatory environment, J. Inflamm. Res. 9 (2016) 231–240.
[73] Y. Zhang, M. Chopp, X.S. Liu, M. Katakowski, X. Wang, X. Tian, D. Wu, Z.G. Zhang, Exosomes derived from mesenchymal stromal cells promote axonal growth of cortical neurons, Mol. Neurobiol. 54 (4) (2017) 2659–2673.
[74] Y.M. Morizawa, Y. Hirayama, N. Ohno, S. Shibata, E. Shigetomi, Y. Sui, J. Nabekura, K. Sato, F. Okajima, H. Takebayashi, H. Okano, S. Koizumi, Reactive astrocytes function as phagocytes after brain ischemia via ABCA1-mediated pathway, Nat. Commun. 8 (2017).
[75] D. Feng, W.L. Zhao, Y.Y. Ye, X.C. Bai, R.Q. Liu, L.F. Chang, Q. Zhou, S.F. Sui, Cellular internalization of exosomes occurs through phagocytosis, Traffic 11 (5) (2010) 675–687.